Chinese Journal of
POLYMER SCIENCE

RESEARCH ARTICLE

https://doi.org/10.1007/s10118-023-3052-x
Chinese J. Polym. Sci. **2024**, *42*, 400–406

Rheological Behaviors of Polymers with Nanoparticles Tethered at Each End

Song-Qi Zhang, Wen-Qing Wang, Jia-Ping Lin*, and Li-Quan Wang*

Shanghai Key Laboratory of Advanced Polymeric Materials, Key Laboratory for Ultrafine Materials of Ministry of Education, School of Materials Science and Engineering, East China University of Science and Technology, Shanghai 200237, China

Electronic Supplementary Information

Abstract The polymer with nanoparticles tethered at each end is a unique model for unraveling the effect of chain ends on the polymer dynamics. We investigated the rheological behavior of this kind of polymer by using nonequilibrium molecular dynamics simulation. The effect of polymer lengths and nanoparticle radii on the complex moduli and viscosity was examined. The dependence of complex moduli on the frequency becomes less pronounced as the polymer is short or the nanoparticle is large. The shear thinning behavior was revealed for these systems, and the scaling exponent of complex viscosity with respect to the frequency was found to change from −1/2 to −3/4 as the polymer shortens or the nanoparticle enlarges. The rheological behavior was further explained by analyzing the mean square distance of nanoparticles. The simulation results were compared with the existing experimental finding, showing an agreement. The work provides information for understanding the chain end effect on polymer rheology.

Keywords Polymer rheology; Modulus; Viscosity; Molecular dynamics

Citation: Zhang, S. Q.; Wang, W. Q.; Lin, J. P.; Wang, L. Q. Rheological behaviors of polymers with nanoparticles tethered at each end. *Chinese J. Polym. Sci.* **2024**, *42*, 400–406.

INTRODUCTION

Polymer composites can have significantly improved properties relative to the neat polymer, which are important for various engineering applications.[1–4] Attaching nanoparticles to the polymers can enhance the miscibility, generating polymer composites with well-defined microstructures and excellent properties.[5–14] One of the methods is to tether the nanoparticle to each end of the polymer (N-P-N), where N and P denote the nanoparticle and polymer, respectively.[15] Because the chain ends can dramatically influence the motion of polymers, the N-P-N could be a unique model for unraveling the end effect on polymer dynamics. As such, understanding the behavior of N-P-N systems is essential to gain insight into the end effects of polymers.

The dynamics of polymer chains with ends of various chemical natures, sizes and mobilities attracted the broad interest of researchers in the past.[16–22] Very recently, Xiong *et al.* synthesized a kind of polyether tethered with polyhedral oligomeric silsesquioxane molecular nanoparticles (MNPs) and explored the chain relaxation and stress response of these polymers.[15] They found that the chain dynamics are impeded by the tethered MNPs, supported by increased viscosity and decelerated diffusion. Wang *et al.* recently conducted a molecular dynamics (MD) simulation on the N-P-N system and examined the effects of nanoparticle radius and polymer length on the glass transition temperature, crystallization temperature, and dielectric properties.[23] It was also shown that the presence of nanoparticles at both ends of the polymer could delay the relaxation of the polymer chain and promote crystallization, resulting in an increase in the glass transition temperature and crystallization temperature of the polymer as the nanoparticle becomes large or the polymer chain shortens.

Of particular importance is the rheological property, as the nanoparticles control the viscoelasticity of nanoparticle-tether polymers. A crucial method to study polymer rheology is the nonequilibrium MD simulation, which was successfully applied to various complex polymer systems.[24–29] For instance, Hong *et al.* employed nonequilibrium MD simulations to elucidate the viscoelastic properties of nanosheet-filled polymer composites and revealed that the polymer composites exhibit an enhanced storage modulus and loss modulus as the nanosheets are loaded.[30] Liu *et al.* used the nonequilibrium MD simulation to explore the shear effect on end-functionalized polymers and found a prominent shear thinning behavior due to the breakage of physical networks.[31] They also discovered that the shear viscosity and shear stress of end-functionalized polymers with bimodal molecular

* Corresponding authors, E-mail: jlin@ecust.edu.cn (J.P.L.)
E-mail: lq_wang@ecust.edu.cn (L.Q.W.)

Received August 6, 2023; Accepted September 8, 2023; Published online October 9, 2023

weight distribution decreases with increasing the proportion of long chains.

In this work, we conducted a nonequilibrium MD simulation on the rheology of the N-P-N systems. The storage and loss moduli were calculated at various strain amplitudes and shear frequencies. Both the effect of the polymer length and nanoparticle radius were explored. Moreover, we examined the diffusion behavior of nanoparticles to gain insight into the dynamics of polymer ends and the mechanism underlying the rheological behaviors. A comparison with existing experimental findings is made, and a good agreement is achieved. The work can shed light on the end effect and rheology of the polymers grafted with nanoparticles.

METHODS

We considered a homopolymer with a nanoparticle tethered at each end. The length of the polymer is N_G, and the radius of the nanoparticle is R. In the molecular dynamics simulation, the polymer is modeled as a spring-bead chain. The radius of the beads and nanoparticles on polymers is determined by the nonbonded interaction potential U_{nb}. The U_{nb} is given as:

$$U_{nb} = 4\varepsilon\left[\left(\frac{\sigma}{r-\Delta}\right)^{12} - \left(\frac{\sigma}{r-\Delta}\right)^{6}\right], \quad r < r_c + \Delta \tag{1}$$

where ε is the energy, σ is the distance, r_c is the cutoff which does not include the Δ distance, meaning that the actual force cutoff is $r_c + \Delta$. The adjacent beads are connected by a spring potential U_b given as:

$$U_b = k_b\left(r - r_{eq}\right)^2 \tag{2}$$

where k_b is the spring constant and r_{eq} is equilibrium bond length. In this work, the values of ε, σ, and r_c are $1.0\varepsilon_0$, $1.0\sigma_0$ and $2.5\sigma_0$, respectively. Note that ε_0 and σ_0 are the units of energy and distance, respectively. In addition, k_b is $100\varepsilon_0/\sigma_0^2$, and r_{eq} is $1.0\sigma_0$ for the bond between polymer beads. The choice of Δ and r_{eq} of the bond connecting the nanoparticle and polymer beads depends on the nanoparticle radius. For example, for the nanoparticle radius of $R = 1.0\sigma_0$, $\Delta = 0.5\sigma_0$, and $r_{eq} = 1.5\sigma_0$ for the bond between the nanoparticle and polymer bead.

All the simulations were implemented with the large-scale atomic/molecular massively parallel simulator (LAMMPS).[32] In the simulation, a $50\sigma_0 \times 50\sigma_0 \times 50\sigma_0$ box with periodic boundary conditions was built, with polymers randomly distributed inside. The initial density is 0.8, and the time step is 0.005τ. Before the calculation of rheological properties, the system is compressed $10^6\tau$ in the *NPT* ensemble, where the pressure and temperature are controlled with the Nose-Hoover barostat and thermostat, respectively.

We employed nonequilibrium MD simulation with an oscillatory shear technique to study the polymer rheology. The "fix deform" function in LAMMPS, conceptually identical to the most widely adopted Lees-Edwards boundary conditions, was applied.[33] An additional velocity is applied to the bead to introduce a shear field. The motion equations of the ith bead are given by the SLLOD algorithm

$$\begin{aligned} \frac{d\mathbf{r}_i}{dt} &= \mathbf{v}_i + \mathbf{e}_x\dot{\gamma}r_{i,y} \\ m_i\frac{d\mathbf{v}_i}{dt} &= \mathbf{f}_i - m_i\mathbf{e}_x\dot{\gamma}v_{i,y} \end{aligned} \tag{3}$$

where $\mathbf{e}_x$ is the normalized vector of the x-component. $\mathbf{f}_i$, $\mathbf{r}_i$, and $\mathbf{v}_i$ are the force, position, and velocity of i^{th} bead, respectively. The stress $\boldsymbol{\sigma}$ was calculated by applying a sinusoidal strain $\gamma(t) = \gamma_0\sin(\omega t)$ to the simulation box,

$$\boldsymbol{\sigma} = \frac{1}{V}\left\langle \sum_i m_i\mathbf{v}_i\mathbf{v}_i + \frac{1}{2}\sum_{i\neq j}\mathbf{r}_{ij}\mathbf{F}_{ij}\right\rangle \tag{4}$$

where γ_0 is the amplitude, ω is the shear frequency, V is the simulation box volume, and $\mathbf{F}_{ij}$ is the force applied on bead j by bead i. The storage modulus G' and loss modulus G'' are given as

$$G' = \frac{\sigma_0}{\gamma_0}\cos(\delta) \tag{5}$$

$$G'' = \frac{\sigma_0}{\gamma_0}\sin(\delta) \tag{6}$$

where σ_0 is the zero-frequency stress, and δ is the phase angle. The more details are given in section 1 of the electronic supplementary information (ESI).

RESULTS AND DISCUSSION

We first examined the dependence of shear moduli on the strain amplitude, with the shear frequency being $0.05\tau^{-1}$. The results are shown in Fig. 1, where the storage moduli G' and loss moduli G'' were plotted against the strain amplitude. As shown, the G' is almost independent of the strain amplitude as the strain is small and decreases as the strain amplitude increases (see Fig. 1a). Moreover, the G' in the linear regime decreases as the chain length N_G increases. While for the G'', the variation is similar to that of G' when the polymer chain is long (N_G=40 and N_G=100) (see Fig. 1b). For the short chain, the G'' first increases and then decreases as the strain amplitude increases. The maximum G'' is reached at the strain amplitude of *ca*. 0.2. Such a phenomenon belongs to the classical Payne effect. As the polymer chain is short, the nanoparticles dominate the microstructure, with the nanoparticles ordered into crystals (for details, see section 2 of ESI). The nanoparticle crystal breaks and recovers as the oscillatory deformation is applied, leading to the Payne effect.[34] In addition, the G'' nearly increases as the polymer chain becomes short.

Note that at the strain amplitude of 10^{-2}, the G'' first decreases, then increases, and finally decreases as the N_G increase. The G'' in the low amplitude primarily responds to the short-distance movement of nanoparticles or polymer beads. Compared to the polymer bead, the free movement of nanoparticles can lead to high energy dissipation and increased G'' due to the large size. Therefore, the G'' could, in principle, decrease as there is a smaller proportion of nanoparticles (*i.e.*, the N_G increases). In addition to the proportion of nanoparticles, the G'' also depends on the mobility of nanoparticles. The reduced mobility of nanoparticles causes decreased energy dissipation and G''. As N_G increases from 10 to 20, although the proportion of nanoparticles decreases, the mobility of nanoparticles significantly increases, resulting in increased G''. This is the reason that the G'' of N_G=10 is smaller in the low amplitude than those of N_G=20 and N_G=40.

Keeping the strain amplitude at 0.05, we investigated the shear moduli as a function of the frequency. Fig. 2(a) shows the plots of storage moduli G' and loss moduli G'' against the frequency. As shown, the N-P-N with N_G=100 exhibits a scaling law characteristic of $G'\sim\omega^{1/2}$ and $G''\sim\omega^{1/2}$. Here, ω is the

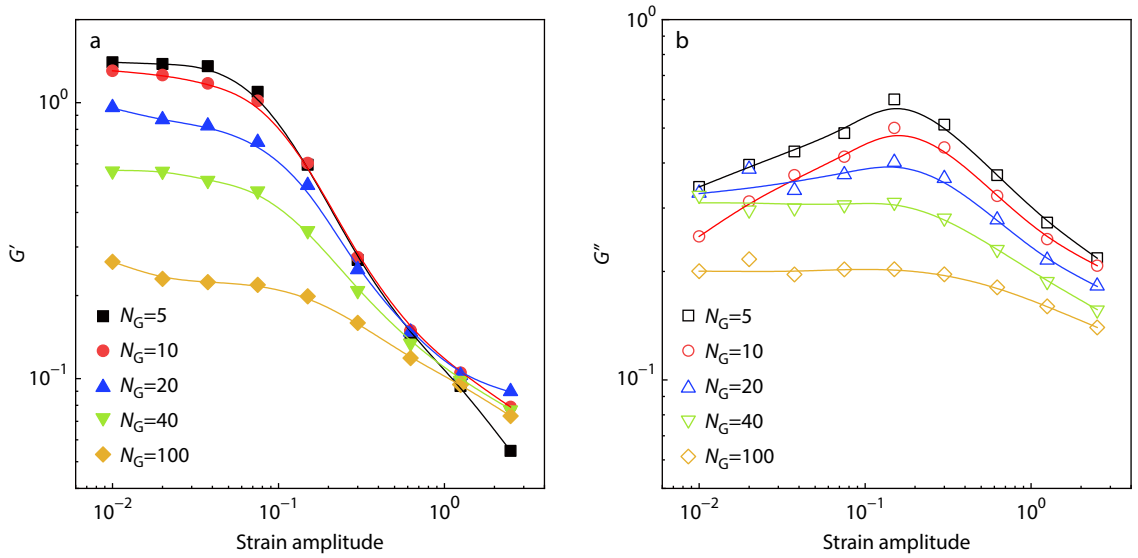

Fig. 1 (a) Storage moduli G' and (b) loss moduli G'' as a function of strain amplitudes for the N-P-N system with various chain lengths, where the nanoparticle radius is $R=1.5\sigma_0$, the reduced temperature is 1.0, and the frequency is $0.01\tau^{-1}$.

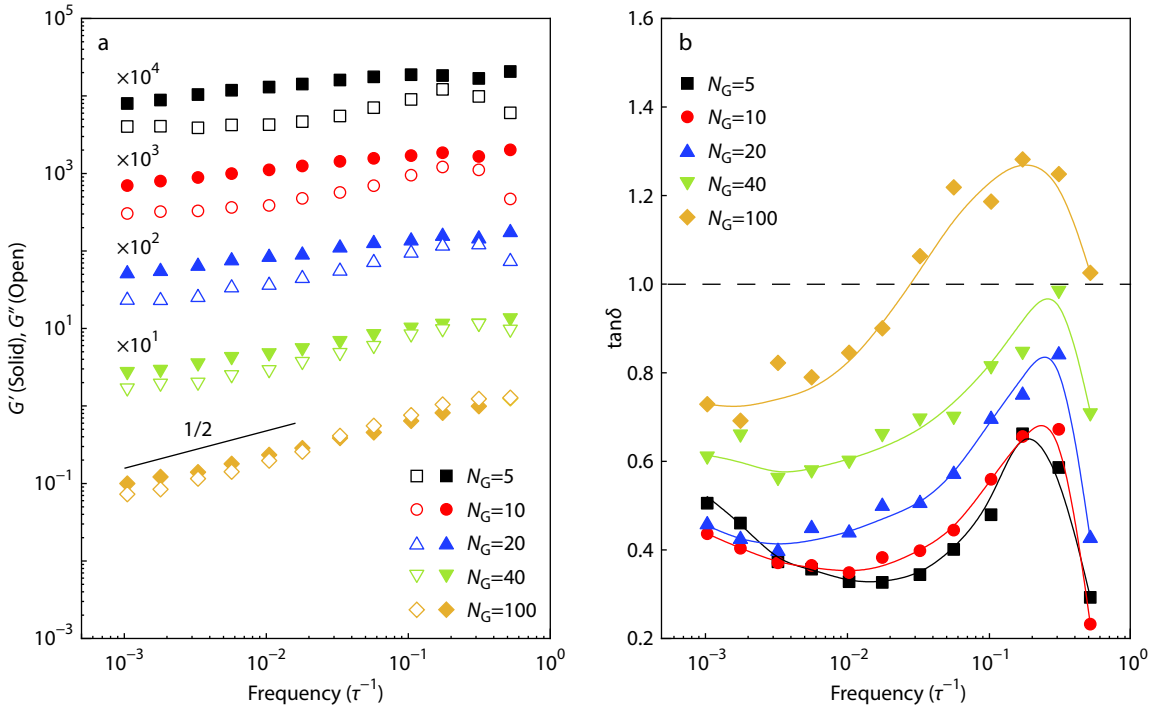

Fig. 2 (a) Storage moduli G', loss moduli G'', and (b) loss tangent tanδ as a function of frequencies for the N-P-N with various chain lengths, where the nanoparticle radius is $R=1.5\sigma_0$, the reduced temperature is 1.0, and the strain amplitude is 0.05.

shear frequency. The terminal flow behavior of $G'\sim\omega^2$ and $G''\sim\omega^1$ was not observed due to the limitation of simulation at lower frequencies. Therefore, the present simulation mainly provides information in the medium frequency regions. The scaling exponent of 1/2 indicates that long N-P-N exhibits the characteristic scaling behavior of the Rouse model. A crossover between G' and G'' occurs at the frequency of *ca.* $0.03\tau^{-1}$. As the N_G decreases, the dependence of G' and G'' on the frequency becomes less pronounced, where the scaling exponent decreases. The modulus plateau ($\sim\omega^0$) appears for the short N-P-N, for example, at $N_G=5$ and $N_G=10$. For the small N_G, the volume of nanoparticles dominates over that of polymer chains, and the nanoparticles are jammed because of insufficient movement space. The G' and G'' approach at the frequency of *ca.* $0.3\tau^{-1}$, after which the G'' tends to decrease.

To gain insight into the crossover behaviors, we also calculated the loss tangent tanδ, which is given as $\tan\delta=G''/G'$. The result is shown in Fig. 2(b). The tanδ shows a peak at the frequency of *ca.* $0.3\tau^{-1}$, but the values are small than 1 except in

https://doi.org/10.1007/s10118-023-3052-x

the case of N_G=100. This implies that the G' is always higher than the G'' in the studied frequency regions, and the N-P-N behaves as a solid. Moreover, the tanδ increases as the N_G increases, indicating the increased mobility of the longer N-P-N. The peak appears at nearly the same frequency, probably attributed to the movement of polymer blocks. As the N_G decrease, the block movement is more significantly impeded by the nanoparticles. This impeding effect leads to a decreased energy dissipation and, therefore, the decreased tanδ.

Fig. 3 shows the plot of complex viscosity η^* as a function of the shear frequency. The η^* is calculated as $\eta^* = \sqrt{\left(\frac{G'}{\omega}\right)^2 + \left(\frac{G''}{\omega}\right)^2}$. One can see from Fig. 3 that the N-P-N shows a shear thinning behavior, where the complex viscosity η^* decreases as the frequency increases. The η^* increases and approaches each other as the N_G decreases. At low frequencies, $\eta^* \sim \omega^{-1/2}$ for long chains and $\eta^* \sim \omega^{-3/4}$ for short chains. These results indicate that in the medium time scales, the longer N-P-N performs as Rouse models, and the short N-P-N behaves like an entangled chain due to the confinement from nanoparticles. At high frequencies, the η^* exhibits a scaling law of $\eta^* \sim \omega^{-1}$, implying that the complex moduli are independent of the frequency.

We recorded the mean-squared distance (MSD) of nanoparticles for N-P-N of various lengths. Fig. 4 shows the temporal variation of the MSD. The MSD appears as a power law of t^2 within a short time due to the ballistic behavior. For a long time, the MSD for all the polymers assumes a scaling feature of MSD$\sim t^{2/3}$, suggesting that the diffusion of nanoparticles at polymer ends obeys a Zimm model. In the intermediate time, the dependence of MSD on the time relies on the polymer chain lengths. The MSD scales as $t^{1/4}$ for short chains, while the MSD is proportional to $t^{3/4}$ for long chains. The power law of MSD$\sim t^{1/4}$ indicates that the polymer chain probably behaves as the entangled chain, which is consistent with the power law for complex viscosity in the same time scale (see Fig. 4).

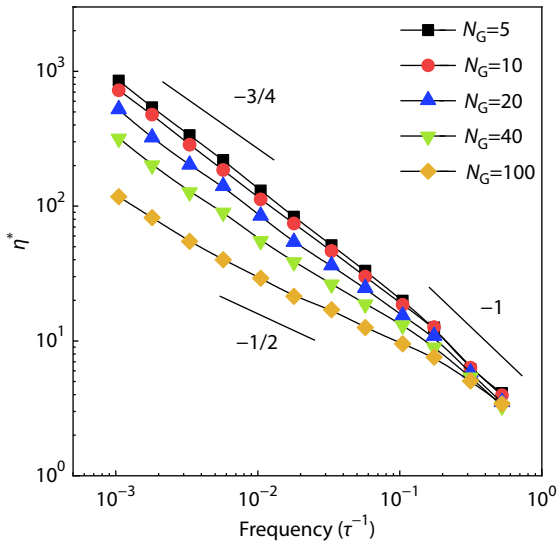

Fig. 3 Complex viscosity η^* versus frequency for the N-P-N with various chain lengths, where the nanoparticle radius is R=1.5σ_0, the reduced temperature is 1.0, and the strain amplitude is 0.05.

In addition to the polymer lengths, we also examined the influence of the nanoparticle size on the viscoelasticity of the N-P-N system. Fig. 5 shows G' and G'' as a function of strain amplitudes for N-P-N with different nanoparticle radii. The N-P-N with small nanoparticles (R=0.5σ_0, 1.0σ_0, and 1.2σ_0) has an evident linear viscoelasticity region, where the moduli are nearly independent of the strain amplitude. As the R increases, the linear viscoelasticity region narrows. For the nanoparticle with R=2.2σ_0, no linear viscoelasticity region of G' was observed in the studied strain amplitude, and the maximum of G'' appears on the curve due to the Payne effect.

Figs. 6(a) and 6(b) show the shear moduli and loss tangent versus the frequency, respectively, for the N-P-N with various nanoparticle radii. As the nanoparticle is small, for R=1.2σ_0, the scaling of G' and G'' with the frequency satisfies the law of $G' \sim \omega^{1/2}$ and $G'' \sim \omega^{1/2}$. The tanδ in the studied frequency is higher than 1 (see Fig. 6b), indicating the G'' is higher than the G'. In this case, the N-P-N with R=1.2σ_0 behaves like a fluid in these shear frequencies. With increasing nanoparticle radii, the dependence of G' and G'' on the frequency becomes less marked. An apparent modulus plateau appears for N-P-N with large nanoparticles, for example, R=2.2σ_0 and R=2.5σ_0. At the frequency of *ca.* 0.3τ^{-1}, the G'' approaches the G' and even surpasses the G' for the system with large nanoparticles. This can be clearly seen from Fig. 6(b) that the tanδ near the frequency of 0.3τ^{-1} is higher than 1. The tanδ peak for $R \geq$1.5σ_0 appears at nearly the same frequency. The peak value first increases and then decreases as the R increases (see Fig. 1b). As the nanoparticles are large, the retarding effect of nanoparticles can increase the energy dissipation of polymers and tanδ values. However, the polymer movement is highly restricted for too large nanoparticles, which leads to decreased energy dissipation.

Fig. 7 shows the complex viscosity η^* versus frequency for N-P-N systems with various nanoparticle radii R. The system exhibits a shear thinning behavior, where the scaling exponent varies from −1/2 to −3/4 as R increases. We also found

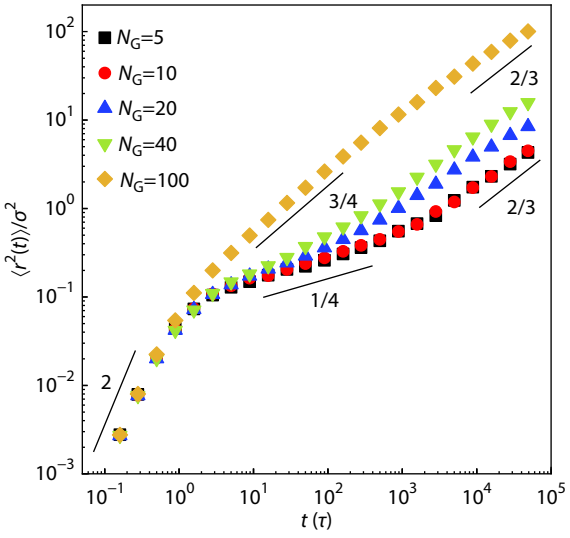

Fig. 4 Temporal variations of mean-squared distances (MSDs) of the nanoparticles of the N-P-N with various chain lengths, where the nanoparticle radius is R=1.5σ_0, and the reduced temperature is 1.0.

https://doi.org/10.1007/s10118-023-3052-x

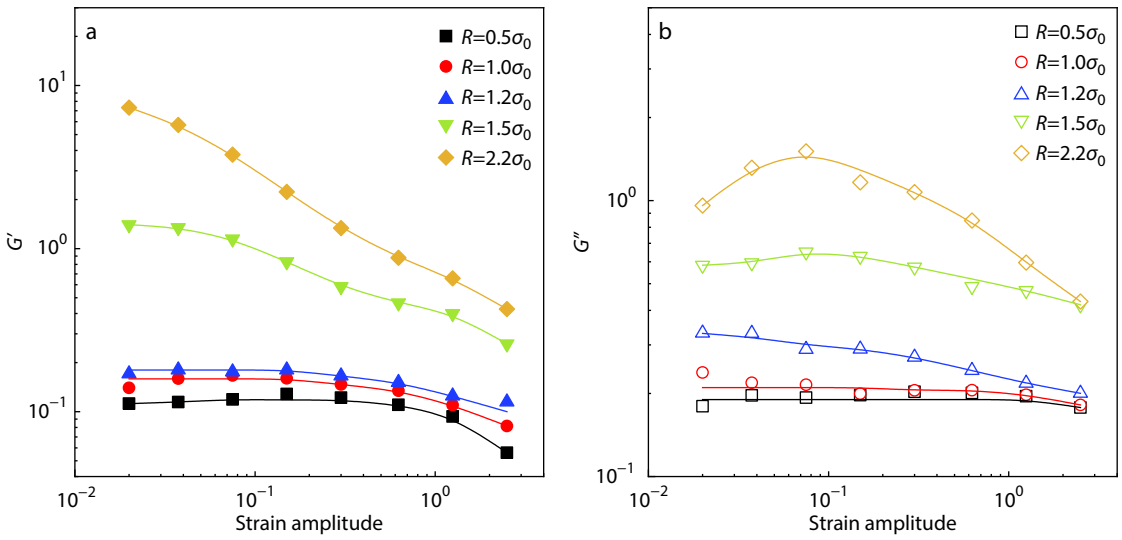

Fig. 5 (a) Storage moduli G' and (b) loss moduli G'' as a function of strain amplitudes for the N-P-N with various nanoparticle sizes, where the polymer length is N_G=40, the reduced temperature is 1.0, and the frequency is $0.01\tau^{-1}$.

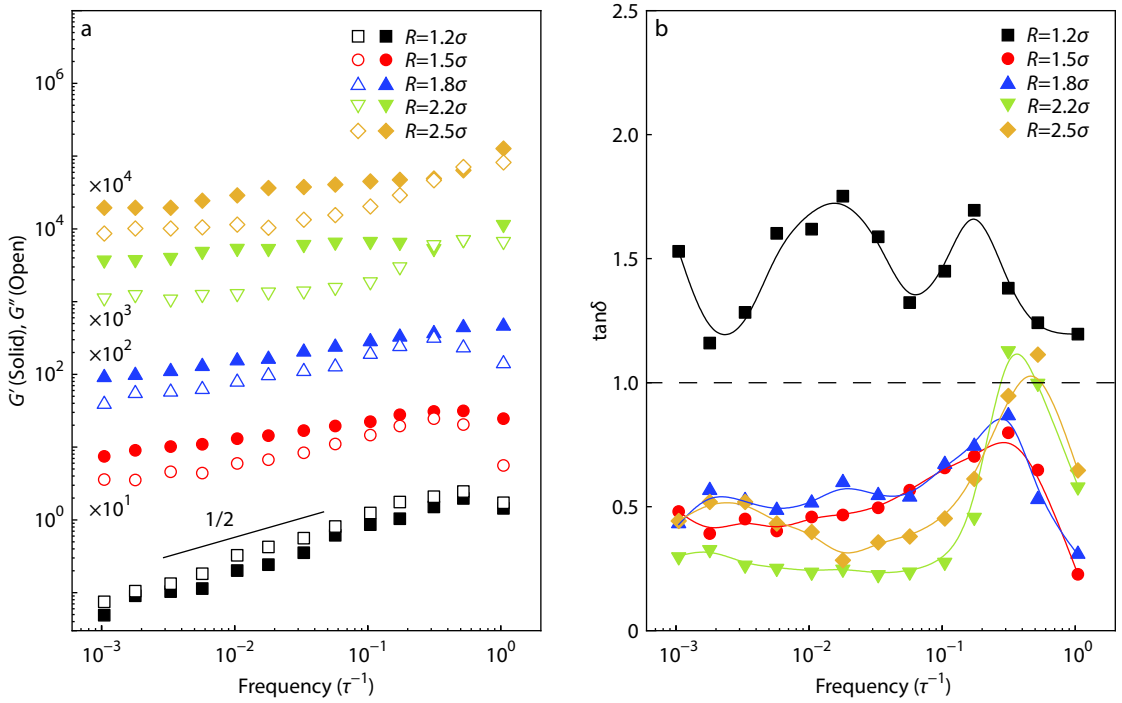

Fig. 6 (a) Storage moduli G', loss moduli G'', and (b) loss tangent tanδ as a function of frequencies for the N-P-N with various nanoparticle sizes, where the polymer length is N_G=40, the reduced temperature is 1.0, and the strain amplitude is 0.05.

that the η^* first increases and then decreases as the R increases. The maximum η^* was found around R=2.2σ_0. Such a phenomenon agrees with the variation of tanδ peaks.

The MSDs for various nanoparticle radii were analyzed, which is shown in Fig. 8. Here, the MSD is rescaled by multiplying the mass of the nanoparticles. From the Fig. 8, one can see that except for R=0.5σ_0, the curves almost coincide within a short time (<10τ), and the difference emerges beyond this time scale. For R=0.5σ_0, the MSD scales with the time as MSD~t^1 in short time and MSD~$t^{2/3}$ in long-time scale. The results indicate that the small nanoparticles diffuse freely as Brownian dynamics in a short time but behave as the Zimm model for a long time due to the chain constraint from polymers. A plateau (~t^0) in the intermediate time scale was observed for R≥1.5σ_0 and prolonged with increasing R values. The appearance of the plateau implies the jamming of nanoparticles. The jamming effect becomes more evident as the nanoparticle radius increases. For example, the nanoparticle of R=2.5σ_0 is highly confined within the time scale of $10^3\tau$. This is the reason why the tanδ and η^* decrease for R=2.5σ_0 as compared with R=2.0σ_0.

The present simulation was compared with the recent experiment carried out by Xiong *et al.*[15] They synthesized a kind of polyether tethered with MNPs and studied the rheolo-

https://doi.org/10.1007/s10118-023-3052-x

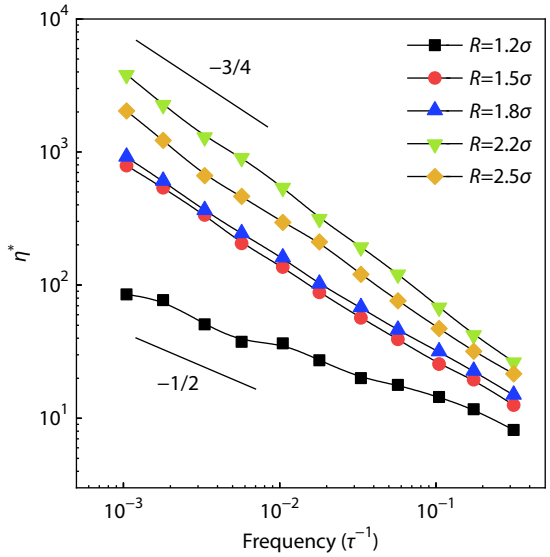

Fig. 7 Complex viscosity η^* versus frequency for nanoparticle-tethered polymers with various nanoparticle sizes, where the polymer length is N_G=40, the reduced temperature is 1.0, and the strain amplitude is 0.05.

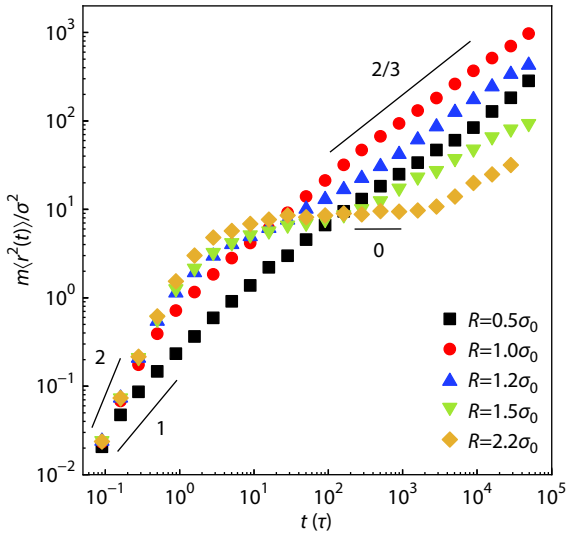

Fig. 8 Temporal variations of mean-squared distances (MSDs) of nanoparticle-tethered polymers with various nanoparticle sizes, where the polymer length is N_G=40, and the reduced temperature is 1.0.

gy of these polymers. They found that the storage and loss moduli of the system exhibited a power law of $G'\sim\omega^{1/2}$ and $G''\sim\omega^{1/2}$ in the medium frequency. This behavior aligns with our observation for P-N-P with long chains (Fig. 2) or small nanoparticles (Fig. 6). Since the difficulty in synthesizing P-N-P with varied nanoparticle sizes, we also observed the phenomenon beyond the experiments. For example, the present work revealed the plateau moduli (Fig. 6) and decreased complex viscosity (Fig. 7) for P-N-P with sufficiently large nanoparticles. Moreover, the work revealed the motion of nanoparticles by calculating the MSD, which is consistent with rheological behaviors. This work can provide additional information on the end effects of P-N-P systems.

CONCLUSIONS

The rheological behavior of N-P-N polymers with nanoparticles tethered at each end was studied by conducting nonequilibrium MD simulations. It was revealed that the nanoparticles at the ends can retard the polymer motion and influence the rheological behavior. The Payne effect was observed for the N-P-N system with small N_G or large R. The dependence of the moduli on the frequency changes from G' (and G'')~$\omega^{1/2}$ to G' (and G'')~ω^0 as the polymer chain shortens or the nanoparticle becomes large. The MSD curve shows that the nanoparticles move slowly as the N_G decreases or R increases, and the significantly large nanoparticles are jammed. The retarding effect of nanoparticles generally leads to increased complex viscosity. However, the complex viscosity decreases for sufficiently large nanoparticles because the chain movement is highly restricted due to the jammed nanoparticles. The work can provide a fundamental understanding of the end effect on the rheology of polymers.

Conflict of Interests

The authors declare no interest conflict.

Electronic Supplementary Information

Electronic supplementary information (ESI) is available free of charge in the online version of this article at http://doi.org/10.1007/s10118-023-3052-x.

ACKNOWLEDGMENTS

This work was financially supported by the National Natural Science Foundation of China (Nos. 21774032 and 51833003) and Shanghai Scientific and Technological Innovation Projects (No. 22ZR1417500).

REFERENCES

1 Balazs, A. C.; Emrick, T.; Russell, T. P. Nanoparticle polymer composites: where two small worlds meet. *Science* **2006**, *314*, 1107–1110.
2 Kumar, S. K.; Benicewicz, B. C.; Vaia, R. A.; Winey, K. I. 50th Anniversary perspective: are polymer nanocomposites practical for applications? *Macromolecules* **2017**, *50*, 714–731.
3 Shukla, P.; Saxena, P. Polymer nanocomposites in sensor applications: a review on present trends and future scope. *Chinese J. Polym. Sci.* **2021**, *39*, 665–691.
4 Yan, M.; Zhang, Y. T.; Wang, X. H. Nanoparticle-filled ABC star triblock copolymers: a dissipative particle dynamics study. *Chinese J. Polym. Sci.* **2023**, *41*, 1462–1476.
5 Lungova, M.; Krutyeva, M.; Pyckhout-Hintzen, W.; Wischnewski, A.; Monkenbusch, M.; Allgaier, J.; Ohl, M.; Sharp, M.; Richter, D. Nanoscale motion of soft nanoparticles in unentangled and entangled polymer matrices. *Phys. Rev. Lett.* **2016**, *117*, 147803.
6 Wang, L.; Ma, J.; Hong, W.; Zhang, H.; Lin, J. Nanoscale diffusion of polymer-grafted nanoparticles in entangled polymer melts. *Macromolecules* **2020**, *53*, 8393–8399.
7 Hu, S. N.; Lin, Y.; Wu, G. Z. Nanoparticle dispersion and glass

transition behavior of polyimide-grafted silica nanocomposites. *Chinese J. Polym. Sci.* **2020**, *38*, 100–108.
8 Medidhi, K. R.; Padmanabhan, V. Diffusion of polymer-grafted nanoparticles in a homopolymer matrix. *J. Chem. Phys.* **2019**, *150*, 044905.
9 Luo, Y. L.; Duan, X. H.; Li, B.; Chen, X. L.; Gao, Y. Y.; Zhang, L. Q. Tuning the electrically conductive network of grafted nanoparticles in polymer nanocomposites by the shear field. *Chinese J. Polym. Sci.* **2020**, *38*, 1426–1434.
10 Ge, T.; Rubinstein, M. Mobility of polymer-tethered nanoparticles in unentangled polymer melts. *Macromolecules* **2019**, *52*, 1536–1545.
11 Hoshino, T.; Murakami, D.; Tanaka, Y.; Takata, M.; Jinnai, H.; Takahara, A. Dynamical crossover between hyperdiffusion and subdiffusion of polymer-grafted nanoparticles in a polymer matrix. *Phys. Rev. E* **2013**, *88*, 032602.
12 Liu, S.; Senses, E.; Jiao, Y.; Narayanan, S.; Akcora, P. Structure and entanglement factors on dynamics of polymer-grafted nanoparticles. *ACS Macro Lett.* **2016**, *5*, 569–573.
13 Lin, C.; Griffin, P. J.; Chao, H.; Hore, M. J. A.; Ohno, K.; Clarke, N.; Riggleman, R. A.; Winey, K. I.; Composto, R. J. Grafted polymer chains suppress nanoparticle diffusion in athermal polymer melts. *J. Chem. Phys.* **2017**, *146*, 203332.
14 Ge, T. Scaling Perspective on dynamics of nanoparticles in polymers: length- and time-scale dependent nanoparticle–polymer coupling. *Macromolecules* **2023**, *56*, 3809–3837.
15 Zhang, X.; Wei, W.; Xiong, H. Hierarchical dynamics of nonsticky molecular nanoparticle-tethered polymers: end and topology effect. *Macromolecules* **2022**, *55*, 3637–3649.
16 Doi, M.; Edwards, S. F. In *The Theory of polymer dynamics*, Oxford University Press: New York, **1988**.
17 Rubinstein, M.; Colby, R. H. In *Polymer Physics*, Oxford University Press: New York, **2003**.
18 Fetters, L. J.; Graessley, W. W.; Hadjichristidis, N.; Kiss, A. D.; Pearson, D. S.; Younghouse, L. B. Association behavior of end-functionalized polymers. 2. Melt rheology of polyisoprenes with carboxylate, amine, and zwitterion end groups. *Macromolecules* **1988**, *21*, 1644–1653.
19 Xing, K.; Tress, M.; Cao, P. F.; Fan, F.; Cheng, S.; Saito, T.; Sokolov, A. P. The role of chain-end association lifetime in segmental and chain dynamics of telechelic polymers. *Macromolecules* **2018**, *51*, 8561–8573.
20 Ge, T.; Rubinstein, M.; Grest, G. S. Effects of tethered polymers on dynamics of nanoparticles in unentangled polymer melts. *Macromolecules* **2020**, *53*, 6898–6906.
21 Lund, R.; Plaza-García, S.; Alegría, A.; Colmenero, J.; Janoski, J.; Chowdhury, S. R.; Quirk, R. P. Polymer Dynamics of well-defined, chain-end-functionalized polystyrenes by dielectric spectroscopy. *Macromolecules* **2009**, *42*, 8875–8881.
22 Miwa, Y.; Yamamoto, K.; Sakaguchi, M.; Sakai, M.; Makita, S.; Shimada, S. Direct detection of high mobility around chain ends of poly(methyl methacrylate) by the spin-labeling. *Macromolecules* **2005**, *38*, 832–838.
23 Wang, W.; Wang, L. Molecular dynamics simulation of polymers with nanoparticles tethered at two ends. *Acta Polymerica Sinica* (in Chinese), **2023**, *54*, 1935–1942.
24 Evans, D. J. Rheology and thermodynamics from nonequilibrium molecular dynamics. *Int. J. Thermophys.* **1986**, *7*, 573–584.
25 Li, Z.; Djohari, H.; Dormidontova, E. E. Molecular dynamics simulations of supramolecular polymer rheology. *J. Chem. Phys.* **2010**, *133*, 184904.
26 Duquesnoy, M., Lombardo, T., Caro, F.; Haudiquez, F.; Ngandjong, A. C.; Xu, J.; Oularbi, H.; Franco, A. A. Functional data-driven framework for fast forecasting of electrode slurry rheology simulated by molecular dynamics. *npj Comput. Mater*. **2022**, *8*, No.161.
27 Nikoubashman, A.; Howard, M. P. Equilibrium dynamics and shear rheology of semiflexible polymers in solution. *Macromolecules* **2017**, *50*, 8279–8289.
28 Zhu, H.; Zhang, S.; Li, X.; Ma, D.; Sun, X.; Wang, Z. H.; Yan, Y.; Xu, J.; Yang, C. Molecular dynamics simulation reveals unique rheological and viscosity–temperature properties of karamay heavy crude oil. *Energy Fuels* **2021**, *35*, 7956–7966.
29 Hong, W.; Lin, J.; Tian, X.; Wang, L. Distinct viscoelasticity of hierarchical nanostructures self-assembled from multiblock copolymers. *Macromolecules* **2020**, *53*, 10955–10963.
30 Hong, W.; Lin, J.; Tian, X.; Wang, L. Viscoelasticity of nanosheet-filled polymer composites: three regimes in the enhancement of moduli. *J. Phys. Chem. B* **2020**, *124*, 6437–6447.
31 Peng, Y.; Yue, T.; Li, S.; Gao, K.; Wang, Y.; Li, Z.; Ye, X.; Zhang, L.; Liu, J. Rheological and structural properties of associated polymer networks studied *via* non-equilibrium molecular dynamics simulation. *Mol. Syst. Des. Eng.* **2021**, *6*, 461–475.
32 LAMMPS Molecular Dynamics Simulator. https://lammps.sandia.gov/. (Accessed August 1 2023).
33 Lees, A.; Edwards, S. The computer study of transport processes under extreme conditions. *J. Phys. C: Solid State Phys.* **1972**, *5*, 1921.
34 Payne, A. R. The dynamic properties of carbon black-loaded natural rubber vulcanizates. Part I. *J. Appl. Polym. Sci.* **1962**, *6*, 57–63.

https://doi.org/10.1007/s10118-023-3052-x